A temperature snapshot from MIS 5c in southeastern Alaska

Paul S. Wilcox[1*], Christoph Spötl[1], R.L. Edwards[2]

[1]Institute of Geology, University of Innsbruck, 6020 Innsbruck, Austria

[2]Department of Earth Sciences, University of Minnesota, Minneapolis, MN, 55455, USA

*Corresponding author: wilcox214@gmail.com

Abstract

Marine Isotope Stage (MIS) 5c, between ~106,000 and ~93,000 years ago, represents an important warm period on Earth in which the current anthropogenic warming can be contextualized. Although viewed as a pronounced interstadial, its climate expression is regionally disparate, with different regions on Earth showing evidence of either cooler conditions than modern-day or warmer conditions than modern-day. It is therefore important to expand temperature reconstructions to different regions on Earth to gain a better picture of climate dynamics during MIS 5c. In Alaska, there are no quantitative temperature reconstructions for MIS 5c, vastly limiting our knowledge of temperature changes in this climatically sensitive high-latitude region. Here, we fill-in this gap by providing the first quantitative temperatures from MIS 5c in Alaska using hydrogen isotopes from fluid inclusions in precisely dated speleothems. We find that regional temperatures during MIS 5c were within error of modern-day (2021 CE) temperatures, likely representing the most recent time period that regional temperatures were as high as modern-day.

1. Introduction

Current warming in northwestern North America is currently approaching or exceeding Holocene maximum values (e.g., *Porter el al., 2019*). To place this warming in context, it is important to extend the regional temperature records to past warm periods. The most recent time period on Earth when temperatures were as warm, or warmer, than present was during certain substages of Marine Isotope Stage (MIS) 5, between ~129 thousand years ago (ka) and ~80 ka. While substage 5e, between ~129 ka and ~118 ka, has received most attention for its exceptional warmth (*Plick et al., 2019; Chadwick et al., 2020; Wilcox et al., 2020*), other substages would benefit from a more thorough temperature evaluation. Substage 5c, between ~106 ka and ~93 ka, is one such substage that also shows evidence of exceptional temperatures compared to modern-day (e.g., *Väliranta et al., 2009*), possibly representing an analog for current warming trends on Earth. However, the shape of MIS 5c from sea-stack data varies greatly, suggesting significant regional spatial variability in temperature (*Lisiecki and Stern, 2016*). It is therefore important to reconstruct temperatures during substage 5c at additional sites across the globe, including northwestern North America.

In Alaska, there are few paleoclimate records from MIS 5 (*Bigelow et al., 2014; Jensen et al., 2016; Farquharson et al., 2018*), and none that definitively capture MIS 5c. Because of this, there are no quantitative temperature reconstructions, leaving a significant void in knowledge from a climatically important region (*Wilcox et al., 2023a*). Here, we fill this gap by incorporating hydrogen isotopes from fluid inclusions in speleothems obtained from southeastern Alaska. The reconstruction represents the first quantitative temperature measurements from MIS 5 from Alaska. Although this record only spans ~2 ka, it provides a robust snapshot that shows temperatures were within error of the modern-day reference at 2021 CE during MIS 5c.

2. Methods

2.1 Site location and sample

Our dataset was developed from one stalagmite retrieved in summer 2023 on Prince of Wales Island, located in the temperate rainforest of the southern Alexander Archipelago in Alaska. Stalagmite EC-23-15-B was found broken on the floor ~60 m inside of El Capitan Cave (56.170 °N, 133.321 °W; 80 m a.s.l.). Klawock, the nearest village to the cave (Fig. 1), has a mean annual air temperature of 7.4 ºC and receives ~2000 mm of precipitation annually.

2.2 U-Th ages

Given that the stalagmite EC-23-15-B is only ~11 cm in length (Fig. 1), only two subsamples were manually drilled for U-Th dating under a laminar flow hood (Table 1). U-Th samples were processed at the University of Minnesota Trace Metal Isotope Geochemistry Lab and analysed using a ThermoFisher Neptune Plus multi-collector inductively coupled plasma mass spectrometer equipped with an Aridus desolvation nebulizer, following the method of (*Shen et al., 2012*). Ages are reported with 2σ errors in years BP. A time-depth model was created in OxCal 4.4 using the Bayesian approach (*Bronk Ramsey, 2008; Bronk Ramsey, 2009; Bronk Ramsey & Lee, 2013*).

2.3 Stable isotopes

A total of 105 stable isotope locations were drilled in stalagmite EC-23-15-B using a Merchantek micromill. Samples were drilled every 1 mm, yielding a temporal resolution of ~15 years. Stable isotope samples were analysed at the University of Innsbruck using a ThermoFisher Delta V isotope ratio mass spectrometer equipped with a Gasbench II (*Spötl, 2011*). Stable isotopes are reported in per mil relative to Vienna Peedee Belemnite (VPDB). Long-term analytical precision is less than or equal to 0.08‰ for both $\delta^{13}C$ and $\delta^{18}O$ (1σ).

2.4 Fluid inclusions

Speleothem fluid inclusion water isotopes (Table 2) were analysed at the University of Innsbruck using a continuous-flow technique via high-temperature reduction on glassy carbon (*Dublyansky & Spötl, 2009*). δ^2H values are given in per mil (‰) using the standard delta notation and are reported relative to Vienna Standard Mean Ocean Water (VSMOW). We extracted 6 calcite blocks, weighing between 1 and 1.5 g, from the central growth axis of stalagmite EC-23-15-B (Fig. 1). The precision of replicate measurements of the in-house calcite standard was typically 1.5‰ for δ^2H for water amounts between 0.1 and 1 μl. Because crushing of the samples released up to 1.9 μl of water (mean 1 μl), the precision of 1.5‰ for δ^2H was found to be adequate for this study.

The paleotemperature record was reconstructed based on the modern-day regional water isotope-temperature relationship (*Rozanski et al., 1992*). Only δ^2H values were used for calculating paleotemperatures for the following reasons: post-depositional processes can alter the original $\delta^{18}O$ in fluid inclusion water (fi) and thus limit the use of $\delta^{18}O_{fi}$ for paleotemperature calculations (*McDermott, 2004*). In addition, δ^2H is not affected by isotopic fractionation during calcite precipitation and remains unaltered as there is no hydrogen source once the water is entrapped in the calcite matrix. We used the global meteoric water line ($\delta^2H = 8*\delta^{18}O + 10$) to convert δ^2H to $\delta^{18}O_{calculated}$. Modern-day drip-water from Wishbone Cave yielded a $\delta^{18}O$ value of –10 ‰ which was used as the modern-day $\delta^{18}O$ anchor point. Fluid inclusion $\delta^{18}O_{calculated}$ values were subtracted from this modern-day $\delta^{18}O$ anchor point to obtain $\delta^{18}O_{difference}$. Next, a temperature-$\delta^{18}O$ transfer function (TF) was used to convert $\delta^{18}O_{difference}$ into temperature. Because it is unclear which TF is appropriate, we evaluated a range of possible values, between 0.26 and 0.36 ‰/°C, which represents the error range of the south-central Alaska temperature-

$\delta^{18}O$ slope of 0.31 ‰/°C (*Bailey et al., 2019*). Because there is only a minor 0.1 °C difference in temperatures calculated from the range of TF values, we report temperatures based on the TF of 0.31 ‰/°C. Finally, we subtracted the mean annual temperature of a nearby weather Station in Klawock (55.555° N, 133.096° W; 24 m a.s.l.) of 7.4 °C (Western Regional Climate Center) to obtain paleotemperature values:

$$T\ (°C) = 7.4 - [-10 - \delta^{18}O_{calculated}]*TF \qquad \text{(Eq. 1)}$$

As the sea-level history is controversial for this time period, with studies showing relative sea level both above and below modern-day during MIS 5c (e.g., *Wainer et al., 2017*), we assume relative sea level was similar to modern-day and applied no sea-level correction.

Uncertainties reflect isotope measurement errors, and one standard deviation of all measurements. The uncertainties were applied through all steps of the paleotemperature calculation. Further, uncertainties were propagated between sampling locations.

3. Results

U-Th ages constrain the timing of growth of speleothem EC-23-15-B between ~103-105 ka. Fluid-inclusion temperatures results show constant temperatures throughout the time interval, varying by less than ~0.1 °C and averaging 7.5 °C (Fig. 2). $\delta^{18}O$ values also vary little throughout the record, ranging between 8.6 ‰ and 9.6 ‰, but with a noticeable decrease at ~104 ka (Fig. 2).

4. Discussion

Our results show exceptional warmth during a brief interval of MIS 5c, within error of regional modern-day warmth (Fig. 2). Therefore, MIS 5c likely represents the most recent time period that regional temperatures were as high as modern-day. Although the substage MIS 5c is generally shown to have interstadial climate conditions based on a global sea stack (*Lisiecki and Stern, 2016*), we were surprised to find temperatures as high as modern-day given that temperatures, for instance, from Greenland show temperatures were ~6 °C cooler than modern-day between 103-104 ka (*Kindler et al., 2014*). Additionally, Greenland temperatures exhibit rapid fluctuations of 10 °C between 104-105 ka (*Kindler et al., 2014*) that are not observed in southeastern Alaska. Temperatures are also significantly cooler in Antarctica, with reconstructions showing MIS 5c was ~3 °C than modern-day (*Petit et al., 1999*). On the other hand, in Scandinavia, summer temperatures show warmer-than-modern temperatures during MIS 5c, upwards of ~3 °C warmer than modern-day (*Väliranta et al., 2009*). While Alaska contains scant evidence of climate conditions during MIS 5c to compare our results, a speleothem record from the Great Basin, USA, shows paleoclimate conditions during MIS 5c, represented by $\delta^{18}O$ values, that are nearly identical to MIS 5e (*Lachniet et al., 2014*), possibly implying temperatures during MIS 5c were near present-day values. These results indicate significant global temperature disparity during MIS 5c, consistent with the regional sea-stack data (*Lisiecki and Stern, 2016*).

In addition to high temperatures during MIS 5c, there is evidence of a strengthened Aleutian Low compared to modern-day based on the exceptionally depleted $\delta^{18}O$ values (Fig. 2). The $\delta^{18}O$ values are consistent with modern-day $\delta^{18}O$ values, which are abnormal relative to the Holocene (*Wilcox et al., 2023b*), and interpreted to represent a dominating meridional moisture source and increased precipitation in southeastern Alaska as a result of a strengthened Aleutian Low (*Wilcox et al., 2023b*). This indicates the presence of an El Niño-like mean state during MIS 5c, which is associated with a strengthened Aleutian Low (*Wilcox et al., 2023b*).

Given that both temperature values from the fluid inclusions and precipitation values from oxygen isotopes are within error of modern-day values during MIS 5c, this offers an interesting view into potential future regional climate trends with increased global warming. We might expect the Aleutian Low to strengthen with increasing warmth and cause more regional precipitation, consistent with modeling results (*Lader et al., 2020*). This warm/wet scenario will likely lead to accelerated glacier loss in the region.

5. Conclusion

Our speleothem fluid inclusion temperature data show that temperatures in southeastern Alaska were within error of modern-day (2021 CE) values. This implies that MIS 5c was likely the most recent time that temperatures were as high as modern-day. When comparing to other records, both regionally and globally, there does not appear to be a consistent temperature trend during MIS 5c when compared to modern-day, with records showing both warmer-than-modern-day and cooler-than-modern-day temperatures. In the future, it will be vital to continue expanding temperature reconstructions during MIS 5c to other regions to better understand the cause of this global temperature disparity.

References

Bigelow, N.H., Edwards, M.E., Elias, S.A., Hamilton, T.D. & Schweger, C.E. (2014). Tundra and boreal forest of interior Alaska during terminal MIS 6 and MIS 5e. *Vegetation History and Archaeobotany*, *23*, 177–193.

Bronk Ramsey, C. (2008). Deposition models for chronological records. *Quaternary Science Reviews*, *27*, 42–60.

Bronk Ramsey, C. (2009). Bayesian analysis of radiocarbon dates. *Radiocarbon*, *51*, 337–360.

Bronk Ramsey, C. & Lee, S. (2013). Recent and planned developments of the program OxCal. *Radiocarbon*, *55*, 720–730.

Chadwick, M., Allen, C.S., Sime, L.C. & Hillenbrand, C.D. (2020). Analysing the timing of peak warming and minimum winter sea-ice extent in the Southern Ocean during MIS 5e. *Quaternary Science Reviews*, *229*, 106134.

Cheng, H., Edwards, R.L., Shen, C.C., Polyak, V.J., Asmerom, Y., Woodhead, J., Hellstrom, J., Wang, Y., Kong, X., Spötl, C. & Wang, X. (2013). Improvements in ^{230}Th dating, ^{230}Th and ^{234}U half-life values, and U–Th isotopic measurements by multi-collector inductively coupled plasma mass spectrometry. *Earth and Planetary Science Letters*, 371, 82–91.

Dublyansky, Y. V. & Spötl, C. (2009). Hydrogen and oxygen isotopes of water from inclusions in minerals: design of a new crushing system and on-line continuous-flow isotope ratio mass spectrometric analysis. *Rapid Communications in Mass Spectrometry, 23*, 2605–2613.

Farquharson, L., Mann, D., Rittenour, T., Groves, P., Grosse, G. & Jones, B. (2018). Alaskan marine transgressions record out-of-phase Arctic Ocean glaciation during the last interglacial. *Geology*, *46*, 783–786.

Jaffey, A.H., Flynn, K.F., Glendenin, L.E., Bentley, W.T. & Essling, A.M. (1971). Precision measurement of half-lives and specific activities of ^{235}U and ^{238}U. *Physical Review C*, *4*, 1889.

Jensen, B.J., Evans, M.E., Froese, D.G. & Kravchinsky, V.A. (2016). 150,000 years of loess accumulation in central Alaska. *Quaternary Science Reviews*, *135*, 1–23.

Kindler, P., Guillevic, M., Baumgartner, M., Schwander, J., Landais, A., & Leuenberger, M. (2014). Temperature reconstruction from 10 to 120 kyr b2k from the NGRIP ice core. *Climate of the Past*, *10*, 887–902.

Lachniet, M.S., Denniston, R.F., Asmerom, Y. & Polyak, V.J. (2014). Orbital control of western North America atmospheric circulation and climate over two glacial cycles. *Nature Communications*, *5*, 3805.

Lader, R., Bidlack, A., Walsh, J.E., Bhatt, U.S. & Bieniek, P.A. (2020). Dynamical downscaling for southeast Alaska: Historical climate and future projections. *Journal of Applied Meteorology and Climatology*, *59*, 1607–1623.

Lisiecki, L.E. & Stern, J.V. (2016). Regional and global benthic $\delta^{18}O$ stacks for the last glacial cycle. *Paleoceanography*, *31*, 1368–1394.

McDermott, F. (2004). Palaeo-climate reconstruction from stable isotope variations in speleothems: a review. *Quaternary Science Reviews*, *23*, 901–918.

Petit, J.R., Jouzel, J., Raynaud, D., Barkov, N.I., Barnola, J.M., Basile, I., Bender, M., Chappellaz, J., Davis, M., Delaygue, G. & Delmotte, M. (1999). Climate and atmospheric history of the past 420,000 years from the Vostok ice core, Antarctica. *Nature*, *399*, 429–436.

Plikk, A., Engels, S., Luoto, T.P., Nazarova, L., Salonen, J.S. & Helmens, K.F. (2019). Chironomid-based temperature reconstruction for the Eemian Interglacial (MIS 5e) at Sokli, northeast Finland. *Journal of Paleolimnology*, *61*, 355–371.

Porter, T.J., Schoenemann, S.W., Davies, L.J., Steig, E.J., Bandara, S. & Froese, D.G. (2019). Recent summer warming in northwestern Canada exceeds the Holocene thermal maximum. *Nature Communications*, *10*, 1631.

Rozanski, K., Araguas-Araguas, L. & Gonfiantini, R. (1992). Relation between long-term trends of oxygen-18 isotope composition of precipitation and climate. *Science*, *258*, 981–985.

Shen, C.C., Wu, C.C., Cheng, H., Edwards, R.L., Hsieh, Y.T., Gallet, S., Chang, C.C., Li, T.Y., Lam, D.D., Kano, A. & Hori, M. (2012). High-precision and high-resolution carbonate ^{230}Th dating by MC-ICP-MS with SEM protocols. *Geochimica et Cosmochimica Acta*, *99*, 71–86.

Spötl, C. (2011). Long-term performance of the Gasbench isotope ratio mass spectrometry system for the stable isotope analysis of carbonate microsamples. *Rapid Communications in Mass Spectrometry*, *25*, 1683–1685.

Väliranta, M., Birks, H.H., Helmens, K., Engels, S. & Piirainen, M. (2009). Early Weichselian interstadial (MIS 5c) summer temperatures were higher than today in northern Fennoscandia. *Quaternary Science Reviews*, *28*, 777–782.

Wainer, K.A., Rowe, M.P., Thomas, A.L., Mason, A.J., Williams, B., Tamisiea, M.E., Williams, F.H., Düsterhus, A. & Henderson, G.M. (2017). Speleothem evidence for MIS 5c and 5a sea level above modern level at Bermuda. *Earth and Planetary Science Letters*, *457*, 325–334.

Western Regional Climate Center, “Klawock climate summary” (wrcc.dri.edu/).

Wilcox, P.S., Honiat, C., Trüssel, M., Edwards, R.L. & Spötl, C. (2020). Exceptional warmth and climate instability occurred in the European Alps during the Last Interglacial period. *Communications Earth & Environment*, *1*, 57.

Wilcox, P.S., Spötl C., Honkonen J., & Edwards, R.L. (2023a). A Walker switch mechanism driving millennial-scale climate variability. *The Innovation Geoscience*, 1, 100026.

Wilcox, P.S., Mudelsee, M., Spötl, C. & Edwards, R.L. (2023b). Solar forcing of ENSO on century timescales. *Geophysical Research Letters*, *50*, e2023GL105201.

Acknowledgments: This work was funded by the Austrian Science Fund (FWF) grant P338960 to P.S.W. We are grateful for the Anna Harris, Jim Baichtal, Christian DeCelle, and the Tongass National Forest Geology program for their continued support for this work. Additionally, extensive stable isotope sampling used in this manuscript was conducted by Jessica Honkonen.

Data availability: Speleothem $\delta^{18}O$ data will be made available on the NOAA server. We have provided an excel file of the fluid inclusion data in the meantime.

Competing interests: There are no competing interests.

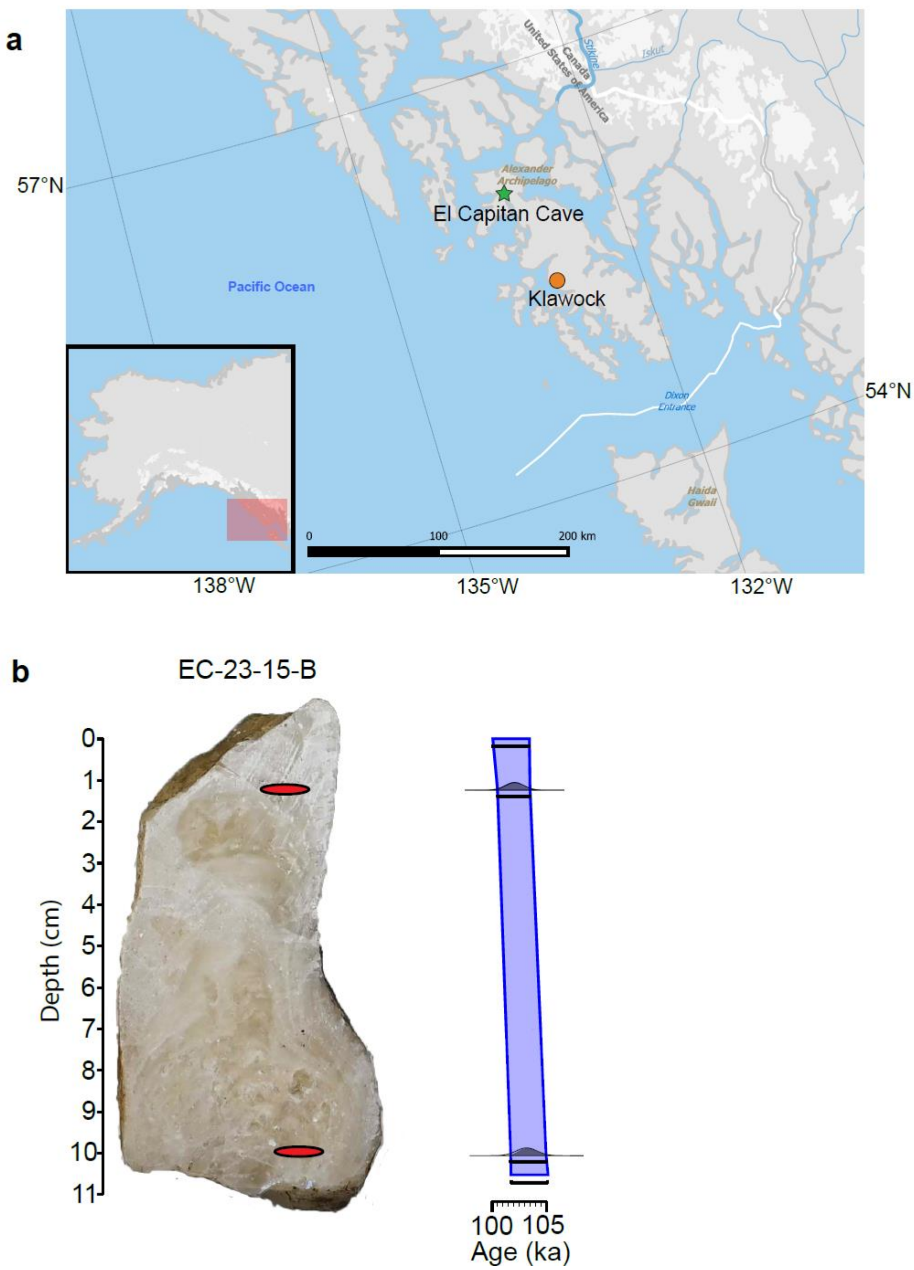

Fig. 1: Speleothem sample site information. (**a**) Map of location of El Capitan Cave, where speleothem EC-23-15-B was retrieved. (**b**) Photo of speleothem EC-23-15-B with U-Th sample locations (red ellipses) and corresponding age depth model.

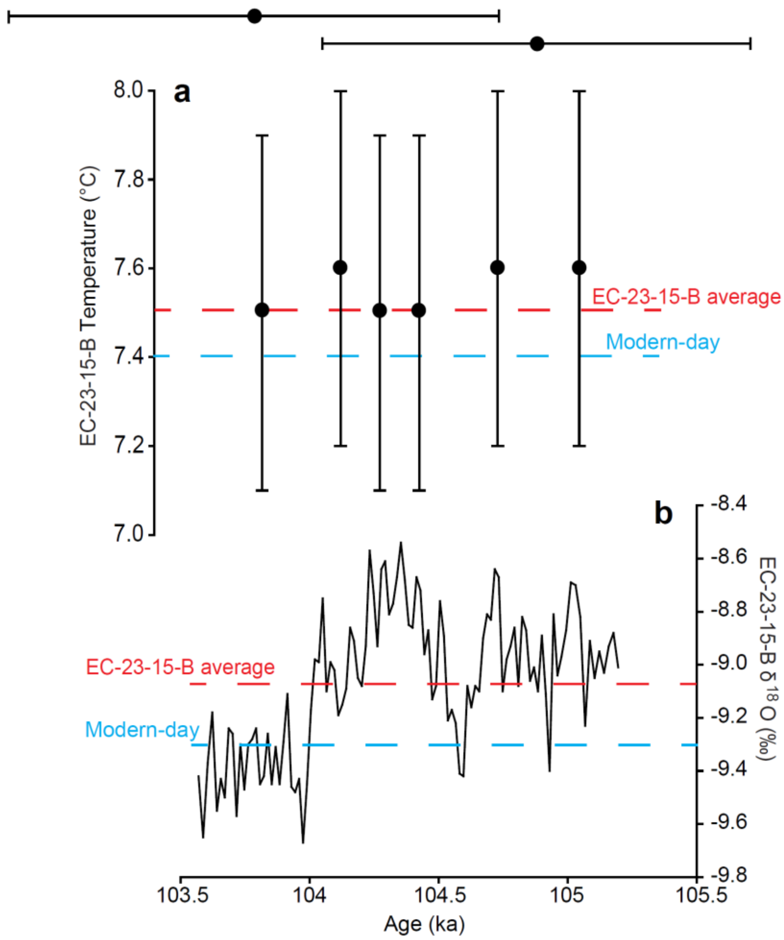

Fig. 2: Speleothem EC-23-15-B fluid inclusion and $\delta^{18}O$ results. (**a**) EC-23-15-B fluid inclusion temperature results. (**b**) EC-23-15-B $\delta^{18}O$ results. Red dashed line represents EC-23-15-B averages, while blue dashed line represents modern-day (2021 CE) conditions. Error bars at the top of figure are U-Th age errors.

Table 1: ^{230}Th dating results. The error is 2s error.

Sample Number	^{238}U (ppb)	^{232}Th (ppt)	^{230}Th / ^{232}Th (atomic x10^{-6})	d^{234}U* (measured)	^{230}Th / ^{238}U (activity)	^{230}Th Age (yr) (uncorrected)	^{230}Th Age (yr) (corrected)	d^{234}U$_{Initial}$** (corrected)	^{230}Th Age (yr (corrected)
367	107.5 ±0.3	331 ±7	4115 ±85	221.2 ±2.9	0.7687 ±0.0039	103918 ±954	103849 ±955	296 ±4	**103780 ±955**
366	138.5 ±0.3	2132 ±43	816 ±17	201.9 ±2.4	0.7615 ±0.0031	105302 ±799	104949 ±834	272 ±3	**104880 ±834**

U decay constants: l_{238} = 1.55125x10^{-10} (Jaffey et al., 1971) and l_{234} = 2.82206x10^{-6} (Cheng et al., 2013). Th decay constant: l_{230} = 9.1705x10^{-6} (Cheng et al., 2013).

*d^{234}U = ([^{234}U/^{238}U]$_{activity}$ – 1)x1000. ** d^{234}U$_{initial}$ was calculated based on ^{230}Th age (T), i.e., d^{234}U$_{initial}$ = d^{234}U$_{measured}$ x e^{l234xT}.

Corrected ^{230}Th ages assume the initial ^{230}Th/^{232}Th atomic ratio of 4.4 ±2.2 x10^{-6}. Those are the values for a material at secular equilibrium, with the bulk earth ^{232}Th/^{238}U value of 3.8. The errors are arbitrarily assumed to be 50%.

***B.P. stands for “Before Present” where the “Present” is defined as the year 1950 A.D.

Table 2: Fluid Inclusion results.

Sample Number	Age (ka)	calibrated (‰ VSMOW)	Transfer Functions (‰/ °C)			error (°C)	δ18O$_{calculated}$ (‰ VSMOW)
			0.31	0.26	0.36		
EC100ka-1	105.1	-65.06	**7.6**	7.6	7.6	± 0.4	-9.4
EC100ka-2	104.8	-64.78	**7.6**	7.6	7.6	± 0.4	-9.3
EC100ka-3	104.6	-67.38	**7.5**	7.5	7.5	± 0.4	-9.7
EC100ka-4	104.3	-67.72	**7.5**	7.5	7.5	± 0.4	-9.7
EC100ka-5	104	-65.27	**7.6**	7.6	7.6	± 0.4	-9.4
EC100ka-6	103.7	-67.24	**7.5**	7.5	7.5	± 0.4	-9.7